Reactive and Functional Polymers 215 (2025) 106382

Contents lists available at ScienceDirect

Reactive and Functional Polymers

journal homepage: www.elsevier.com/locate/react

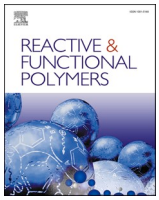

Eu-modified poly (L-lactic acid) microspheres with enhanced crystallinity and stability by incorporation of rare-earth ions interacting with polymer chains via temperature-tuned emulsification

Giulia Tamburini [a], Fabian Gasser [b], Eduardo Machado Charry [b], Roland Resel [b], Giulia Tarricone [a], Sergio Piva [a], Adele Sassella [a], Roberto Lorenzi [a,*], Alberto Paleari [a]

[a] Department of Materials Science, University of Milano-Bicocca, Via Cozzi 55, 20125 Milano, Italy
[b] Institute of Solid State Physics, Graz University of Technology, Petersgasse 16/II, 8010 Graz, Austria

ARTICLE INFO

Keywords:
Poly (lactic acid)
Microspheres
Europium
Rare-earth ions
Spectroscopy

ABSTRACT

Incorporation of lanthanide ions into polymers via rare-earth organic complexes poses the issue of the interaction between the polymer matrix and lanthanide compounds, which can significantly influence both the rare-earth functional properties and the structural features of the matrix. This work investigates the synthesis of europium-containing poly (L-lactic acid) (PLLA) microspheres through an oil-in-water emulsion of PLLA and europium (III) acetylacetonate hydrate dissolved in dichloromethane and water containing poly (vinyl alcohol). The synthesis was conducted at various temperature – from 20 °C to 80 °C, including conditions above the PLLA glass transition. Results from X-ray diffraction and Raman scattering give evidence of higher crystallinity in Eu-modified PLLA microspheres than in undoped PLLA, while differential scanning calorimetry indicates that Eu addition hinders PLLA chain mobility with a resulting decrease in PLLA melt crystallization ability. Insights into the incorporation mechanisms of Eu^{3+} in the microspheres were provided by photoluminescence, scanning-electron-microscopy, micro-computed-tomography, X-ray fluorescence, and infrared spectroscopy. The analysis shows that Eu^{3+} complexes enter the polymer structure by interacting with PLLA chains, modifying the local environment of the lanthanide ions. These findings finally provide a new basis for designing tailored synthesis methods for specific applications.

1. Introduction

Polymers with encapsulated lanthanide compounds are currently studied for their potential in many applications, including LED displays [1,2], transparent films for luminescent solar concentrators [3], light-conversion coatings in solar cells [4], optical sensors of thermochemical parameters [5,6], and microspheres containing radioisotopes for internal radiotherapy [7–10]. The local environment of the functional ions – used as light-emitters or activatable radioisotopes, depending on the application – is significantly influenced by the specific choice of lanthanide compound used in the polymer functionalization process. The lanthanide compound can, indeed, perturbate crystallinity, density, and porosity of the polymer matrix, impacting both the functionality of the system and the chemical and structural stability of the material.

Many studies have been devoted in the last years to investigating the stability of functional and structural properties in lanthanide-containing polymers from different synthesis strategies and precursor compounds [5]. In the field of polymer microspheres for internal radiotherapy, research has focused on aspects with important medical impact, such as the retention of radioactive species, as well as the biocompatibility and biodegradability of the micro-system [8,9]. In this area, poly (L-lactic acid) (PLLA) has emerged as the preferred matrix for medical carriers due to its peculiar properties of biocompatibility. In such systems, biodegradability and radiation hardness – often competitive properties – have been analysed by looking at the time evolution of the morphology of the microcarriers and the release of incorporated species [11,12], either by exposure to irradiation or by degradation in buffer solutions.

The development of reliable medical protocols using polymer-based micro-carriers requires an adequate knowledge of the role of the polymer structure in initiating the mechanisms of radiation-induced damage, as approached in a few works on PLLA from different synthesis and in different ranges of irradiation dose [13,14]. Consequently, in PLLA

* Corresponding author.
E-mail address: roberto.lorenzi@unimib.it (R. Lorenzi).

https://doi.org/10.1016/j.reactfunctpolym.2025.106382
Received 4 April 2025; Received in revised form 30 May 2025; Accepted 13 June 2025
Available online 15 June 2025

microspheres, some studies addressed the dependence of crystallinity and mobile vs. rigid amorphous fraction on the emulsification process, including the percentage of the compound involved and the synthesis temperature [15,16]. Concerning lanthanide-doped polymer systems, lanthanides are typically introduced by means of organic molecules such as acetylacetonate or other chelating molecules [5]. Most investigations have focused on the radiation hardness and lanthanide ion retention properties in microspheres for radiotherapy. Other studies analysed the lanthanide related light emission in polymer and blend films for optical applications prepared by specific synthesis with rare-earth ions.

The aim of the present work is to advance the understanding and control of the mechanisms responsible for the incorporation of Eu in PLLA microspheres using europium (III) acetylacetonate hydrate ($Eu(acac)_3$) via temperature-controlled emulsification processes. The study is focused on determining whether and how the involvement of europium can modify the PLLA properties of crystallinity, degradability, and radiation hardness. Diffractometric, calorimetric and spectroscopic responses are analysed to gain insight into Eu coordination shell and polymer structure. In the following sections, the structural and morphological features of the synthesized material are presented first – analysing microsphere size, PLLA crystallinity, biodegradability, and radiation hardness – looking at the effects of Eu incorporation at different emulsification temperatures. Then, complementary results are presented – from PL and IR spectroscopy and variable-temperature diffractometry – shedding light on how Eu^{3+} ions integrate into PLLA and affect its structure and stability.

2. Materials and methods

Eu-loaded PLLA microspheres were synthesized using an oil-in-water emulsification technique followed by solvent evaporation, based on previously reported protocols [17,18]. The organic phase consisted of 200 mg of bio-produced PLLA (Mw ≈ 84 kDa) obtained from pellet of about 10 mm^3 cut from strings produced via hot extrusion (180 °C) (Galatea Biotech s.r.l., Milan, Italy) and europium (III) acetylacetonate hydrate ($Eu(acac)_3$, ABCR GmbH, Germany) (200 mg). These were dissolved in 10 mL of dichloromethane (DCM, 99 %, VWR Chemicals) under stirring at 20 °C for 10 min until complete dissolution. The aqueous phase was prepared by dissolving 750 mg of polyvinyl alcohol (PVA, Mw ≈ 31 kDa, hydrolysis degree = 88 %, Sigma-Aldrich) in 75 mL of water under continuous stirring at 40 °C. After dissolving the PVA, the organic phase was added to the aqueous phase under mechanical stirring at 500 rpm for two hours, allowing DCM evaporation. The temperature of the aqueous phase (T_{emu}) varied between 20 °C and 80 °C. For $T_{emu} \geq$ 50 °C, given the boiling point of DCM ≈ 40 °C, the organic phase was carefully introduced to minimize foaming. After the synthesis, the microspheres were allowed to cool to room temperature, washed with water to remove excess PVA, and drop cast onto 1 × 1 cm silicon wafers. These were left for at least 8 h to ensure complete solvent evaporation. For degradation kinetics and Eu release studies, the microsphere batches were immersed in phosphate buffer saline solution (PBS, pH 7.4, with 0.05 % TWEEN® 20, Sigma-Aldrich) at 25 °C for 30 days. Aliquots of microspheres were periodically extracted at increasing times (1, 3, 5, 8 h, 1, 2, 3, 4 days; …), with $t = 0$ corresponding to the moment the microspheres were added to the PBS solution and drop cast on 1 × 1 silicon wafers for further analyses. Batches of Eu-PLLA microspheres were exposed to 100 Gy X-ray irradiation using a W-target X-ray tube (20 kV, 20 mA) to investigate possible radiation-induced molecular modification at the conditions previously used to observe the onset of the first stages of the PLLA molecular unit change [14], so as to evaluate enhancement or lowering of the propensity to trigger radiation-induced damage as a function of the synthesis conditions.

Optical microscopy was used to collect wide images for obtaining statistically significant sampling of the microsphere size distribution. Images were collected using a Leica DM LM microscope equipped with a Leica DFC280 digital color camera and a 10× objective to capture images. Scanning electron microscopy (SEM) was used to investigate microsphere surface and internal structure. A Thermo Fisher Phenom G6 SEM operating at 10 kV and equipped with a back-scattered electron detector (BSD) was employed. The cross sections of the microspheres were prepared by embedding them in epoxy resin and cutting them with a lapping machine. Samples were mounted on aluminum stubs with double-sided adhesive carbon tape and vacuum-coated with a thin gold layer.

Micro-computed tomography (micro-CT) analysis was conducted to investigate the internal structure of the Eu-modified microspheres using a UniTOM HR (Tescan Orsay Holding, Brno, Czech Republic) operating in nanofocus mode. The instrument was set to 50 kV accelerating voltage with a target current of 26 μA. For the microspheres to be analysed, they were embedded in epoxy resin and sealed in a polyimide tube (Ø = 1.8 mm) for scanning. Tilt series were acquired at 0.9 μm voxel size over 2286 projections within a 360° range. Projections were recorded using a DELEXA camera with an exposure time of 1500 s, averaging eight frames per projection with 2× binning. No filter was used to harden the beam. Reconstruction was performed using TESCAN Panthera 1.4.4 software, and the data were visualized using ORS Dragonfly software (Version 2024.1, Comet Technologies Canada Inc., Montreal, Canada).

X-ray fluorescence (XRF) spectroscopy was performed to estimate in a semi-quantitative way the amount of europium throughout the degradation process within the samples - both drop-cast microspheres and release waters - with an ARTAX 200 (Bruker) instrument equipped with a molybdenum-anode X-ray tube operating at 40 kV, 600 μA, for a measurement time of 120 s. Evaluation of europium content in the drop cast samples was assessed by calculating the integral of the characteristic fluorescence peak at $L\alpha_1$ energy (5.85 keV). To make the comparison between spectra reliable, they were normalized with respect to Rayleigh scattering (17.4 keV, corresponding to the Kα emission of Mo).

The presence of crystalline phases in the microspheres was estimated with Grazing Incidence X-ray Diffraction (GIXD) measurements were carried out at the SAXS beamline of the Elettra synchrotron in Trieste, employing a 1.54 Å wavelength. Diffraction was detected using a Dectris Pilatus 1 M detector positioned 225 mm from the sample. For calibration, an LaB_6 standard was used. GIXD patterns were recorded in a q range up to 30 nm^{-1} with an incidence angle of $\omega = 0.5°$. Data processing and azimuthal integrations were performed with GIDVis software [19].

To verify the thermal stability of the crystalline phases, Powder X-ray Diffraction (PXRD) analysis was conducted using a PANalytical Empyrean diffractometer with a Cu-Kα source (40 kV, 40 mA). Data were collected over a 2θ range of 5.0°–30.0° at a scan speed of 2.0°/min. Diffraction was detected with a 0.1 mm antiscatter slit/0.02 rad Soller slit configuration and a PANalytical PIXcel detector. In-situ crystallization studies utilized a DHS 900 heating stage (Anton Paar) under inert nitrogen conditions. The crystalline fraction of PLLA was determined by calculating the ratio of the integrated area of the diffraction peaks corresponding to the α-crystalline phase of PLLA to the total integrated intensity of the XRD pattern. This total intensity includes both the contributions from the crystalline peaks and the broad amorphous halo. A fitting procedure was employed to accurately deconvolute and quantify the individual peaks and the amorphous contribution.

Differential Scanning Calorimetry (DSC) measurements were performed using a DSC-1 system (Mettler Toledo STARe) equipped with a liquid N_2 cooling accessory. Samples were sealed in 40 μL aluminum pans, and heat flow was recorded during heating/cooling cycles between 0 °C and 220 °C at 10 °C/min in N_2 atmosphere. Indium was used for temperature and heat flow calibration.

The structures of individual microspheres were examined using Raman spectroscopy with a Labram Horiba Jobin-Yvon spectrometer and a 633 nm (HeNe laser) excitation source. The same instrument setup was employed for photoluminescence (PL) analysis of Eu^{3+} emission spectra, utilizing a 488 nm (Ar^+ ion) laser. Scattered light was collected through a 20× objective on an Olympus BX40 microscope and detected

with a CCD-Sincerity (Jobin-Yvon) system, offering a spectral resolution of 1 cm^{-1}.

FTIR analyses for the investigation of eventual radiation-induced modifications in the vibrational spectra of irradiated and non-irradiated samples were conducted using a Thermo Fisher Nicolet iN10 infrared microscope, spanning 675 to 4000 cm^{-1}. Transmission FTIR was performed with LED illumination on a CVD-deposited diamond substrate.

3. Results and discussion

3.1. Synthesis and treatment effects on microsphere morphology and Eu retention

Fig. 1a–e show representative SEM images of the Eu-modified PLLA synthetized by emulsification at different temperature, confirming the formation of spherical microparticles of a few tens of μm in size. The results of a careful and statistically reliable quantification of the size distribution, from the analysis of wider field-of-view images by optical microscopy (Fig. S1), are reported in Fig. 1f–j. From these data, the microspheres mean size ranges between approximately 60 and 80 μm. This result – with values larger than those reported in pure PLLA microspheres at the same synthesis conditions (in the 30–60 μm range) [15] – points to an enhanced aggregating action on the polymer chains during the formation of the microspheres and the parallel incorporation of europium. Additionally, comparing batches from different synthesis conditions, the microsphere mean size results to be influenced by the emulsification temperature. A moderate increase of microsphere mean size is observed by increasing T_{emu} from room temperature to 50 °C, then to the PLLA glass transition temperature at about 60 °C, and further up to 80 °C.

Higher-resolution SEM images show that the surfaces are compact and smooth in microspheres prepared below the glass transition temperature (Fig. 2a) – with only minor traces of porosity or corrugations at the surface – whereas an increased number of pores and corrugations is observed at the surface of microspheres emulsified at temperatures comparable or higher than 60 °C (Figs. 2b and S2), at which the fast evaporation of DCM during the formation of microspheres can likely play a role. Despite these variations in smoothness or porosity, the observed morphology is characterized by a strong stability, without relevant changes at the end of the investigated degradation treatments (Fig. 2c and d).

The XRF analysis of the different microsphere batches registers a good yield of Eu incorporation. Fig. 3a compares the XRF spectra of a representative sample of Eu-modified PLLA microspheres and $Eu(acac)_3$ as a reference. The characteristic Eu lines indeed display an intensity of the same order of magnitude (about a factor 0.8 lower in PLLA than in $Eu(acac)_3$) and suggest that the Eu concentrations in both systems (about 34 % w/w in $Eu(acac)_3$) are quite similar. Importantly, no detectable evidence of Eu-content decreases in the microsphere samples results from XRF analysis at any step of the degradation treatment (Fig. 3b), since the calculated relative Eu Lα1 peak area shows no significant variations. Moreover, the XRF spectra of dried residuals of the buffer solution show no detectable presence of Eu (data not shown).

In the next section, diffractometric and calorimetric data are presented giving some elements to understand the possible effects on the polymer structure, specifically on PLLA crystallinity and its propensity to crystallization.

3.2. Eu-related effects on the polymer structure

Fig. 4a reports a representative GIXD pattern of an Eu-modified PLLA microsphere sample compared with that collected on a reference Eu-free sample prepared at identical temperature and synthesis procedure. The comparison registers a much lower intensity of the broad unstructured halo at q vector between 7 and 18 nm^{-1} in Eu-modified material.

This result highlights a relevant reduction of the amorphous fraction, likely related to the incorporation of europium; a similar effect is also observed in all Eu-modified microsphere samples with respect to pure PLLA microspheres. Fig. 4b displays the crystalline fraction calculated from the analysis of the GIXD pattern in the whole set of Eu-modified samples prepared at different T_{emu}. As a matter of fact, the lower limit of the range of values of crystalline fraction in Eu-modified microsphere samples aligns closely with the upper limit previously reported in pure PLLA microspheres at the same conditions [15]. Scherrer analysis of the width of the main reflections gives an estimate of the extension of the crystalline domain to be approximately 30 nm for all T_{emu}.

Besides the reduction of the broad amorphous halo, other two relevant differences characterize the GIXD pattern of Eu-modified PLLA microspheres. First, in all Eu-modified samples, an additional reflection is observed in the region of small q, at about 5 nm^{-1} (highlighted in Fig. 4a). Furthermore, a clear shift is registered towards lower q – about 0.13 nm^{-1} – in the main reflections of the PLLA α-phase at about 10, 12, and 13 nm^{-1} (inset of Fig. 4a).

As regards the shift of the PLLA reflections, the result suggests that Eu incorporation takes place by modifying the unit cell in the PLLA crystalline domains, with Eu^{3+} ions truly entering the polymer structure and slightly expanding the cell parameters. About the low-q reflection at 5 nm^{-1} not belonging to the diffraction pattern of PLLA, its origin is undefined, but similar features are reported in other works on Eu-doped polymers [1,4,20]. On the other hand, this diffraction peak does not provide any detailed information on how Eu^{3+} ions are incorporated.

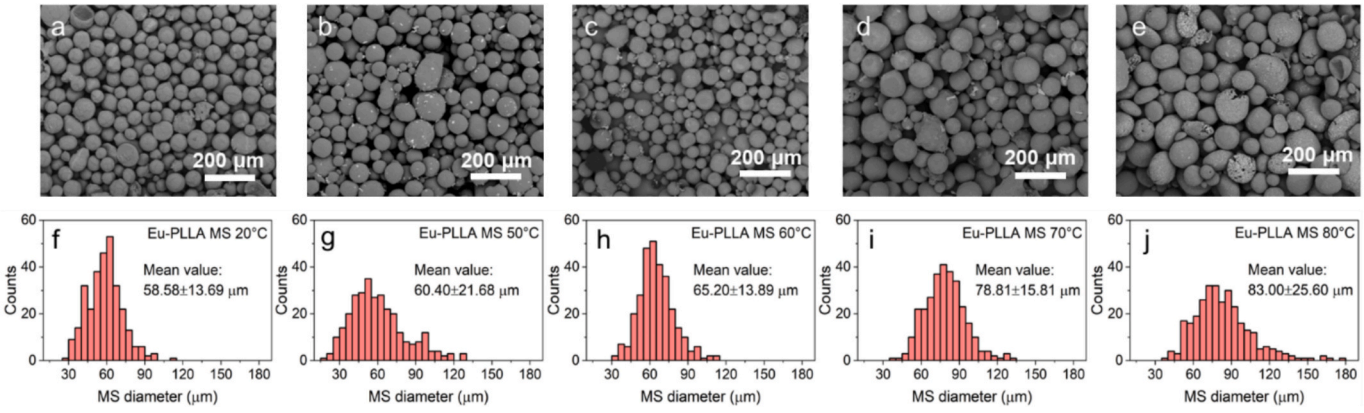

Fig. 1. Size dispersion of Eu-modified PLLA microspheres. (a–e) Representative SEM images of microsphere produced by emulsification at 20, 50, 60, 70, and 80 °C, respectively. (f–j) Histograms of size dispersion in the microsphere batches exemplified by the SEM images in (a–e), respectively, from a large statistical sampling by optical microscopy analysis (see Fig. S1).

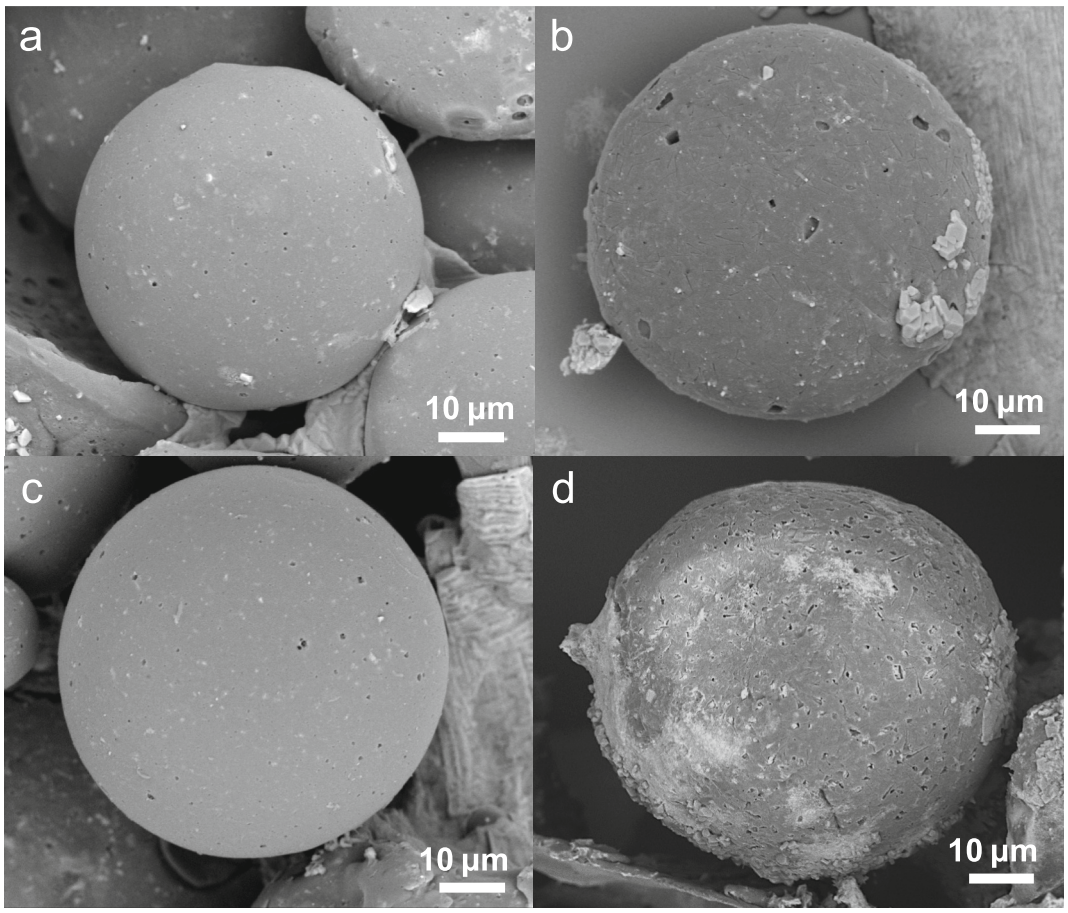

Fig. 2. Eu-modified PLLA microsphere surface vs. emulsification temperature and degradation. (a,b) SEM images of microsphere prepared at 20 °C and a microsphere prepared at 80 °C, respectively. (c,d) SEM images of two microspheres of the batches in (a) and (b), respectively, after treatment in buffer solution for 1 month.

However, some indication can be preliminary argued. The high scattering factor – with intensity comparable with that of the matrix pattern – suggests that the 5 nm^{-1} reflection is related to ordered arrangements of Eu ions, which possess high electron density. The low *q*-value corresponds to a quite large spacing of the diffracting objects (about 1.2 nm), probably determined by the steric effects of the chelating organic groups belonging to the ion coordination shell, as in other polymeric matrixes [1]. Indeed, a diffraction peak at approximately the same position is also present in $Eu(acac)_3$, where the coordination shell involves acetylacetone molecules (curve 3 in Fig. 4a). However, in $Eu(acac)_3$ pattern, the low-q reflection is accompanied by other, more intense diffraction peaks not observed in Eu-modified PLLA. Only with the aid of complementary spectroscopic data, better clarifying the possible environment of Eu^{3+} ions in the investigated microspheres, this issue can be discussed further. Regardless of the specific mechanism of incorporation of europium in the microspheres, the outcome reported in Fig. 4b, with a clear-cut difference in crystallinity at fixed synthesis conditions, poses the question of a possible important role of europium in determining the final PLLA matrix structure within the microspheres. The next section provides further data on this aspect.

3.3. Crystallization propensity

The DSC curves in Fig. 5 register relevant differences between Eu-modified and pure PLLA microspheres. Cold crystallization is almost lacking in Eu-modified batches, with only the sample synthesized at 60 °C – characterized by the most intense amorphous halo in the diffraction pattern – showing higher enthalpy with respect to the reference batch (Fig. S3 in SI). Furthermore, in Eu-modified samples, the cold crystallization peak, when present, lies at a temperature T_{cc} higher than in pure PLLA microspheres. The observed T_{cc} values are indeed quite close to the threshold for melting, whose endothermic peak temperature T_m shifts to lower values, from 175 to 165 °C. In all Eu-modified batches, no evidence is found of bounded water molecules and the melting of segregated $Eu(acac)_3$ at about 102 ($T_{m,1}$) and 140 °C ($T_{m,2}$), respectively (curve 3 in Fig. 5).

The lack of cold crystallization during the first heating in the DSC curve of Eu-modified microspheres cannot necessarily imply a more complete crystallization, but it should be interpreted as the result of an interaction between Eu and PLLA molecules. Such an interaction can indeed restrict the mobility of PLLA molecules and inhibit the occurrence of cold crystallization. As a matter of fact, the subsequent cooling and second heating in the DSC curve confirm this interpretation. During the cooling process, the DSC curve of Eu-modified PLLA does not show crystallization exotherm peak, as expected from reduced mobility of PLLA molecules caused by interactions between Eu and PLLA molecules. During the second heating, when pure PLLA exhibits nearly identical curve to the first heating, the cold crystallization peak of Eu-modified PLLA is almost undetectable, and the melting peak is also very small, indicating that the crystallinity is quite low. All the above facts indeed demonstrate that the addition of Eu reduces PLLA crystallization capacity, despite the fact that Eu incorporation improves PLLA crystallization during emulsification.

Fig. 6a and b display the PXRD patterns of a representative sample of Eu-modified microspheres during heating from room temperature to 180 °C. Above T_m the low q-value (5 nm^{-1}) peak does not show any change at intermediate temperature, specifically at 130 °C, corresponding to the T_m of $Eu(acac)_3$. This additional diffraction peak

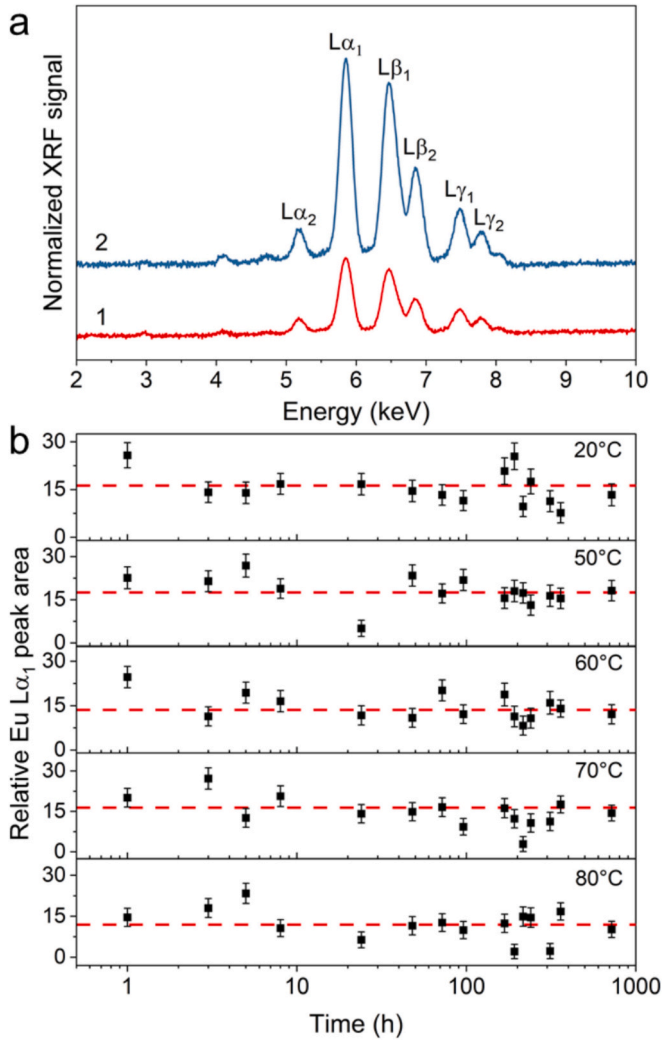

Fig. 3. Microsphere Eu content and release. (a) XRF spectra in the region of Eu transitions in an Eu-modified PLLA microsphere sample (curve 1 in red) and in a reference sample of $Eu(acac)_3$ (curve 2 in blue) normalized to the maximum of curve 2. (b) Integrated intensity of the $L\alpha_1$ XRF peak in PLLA microsphere drop cast aliquots measured after different time of stay in PBS. The red dashed lines represent the mean value of the integrated intensity over time. (For interpretation of the references to color in this figure legend, the reader is referred to the web version of this article.)

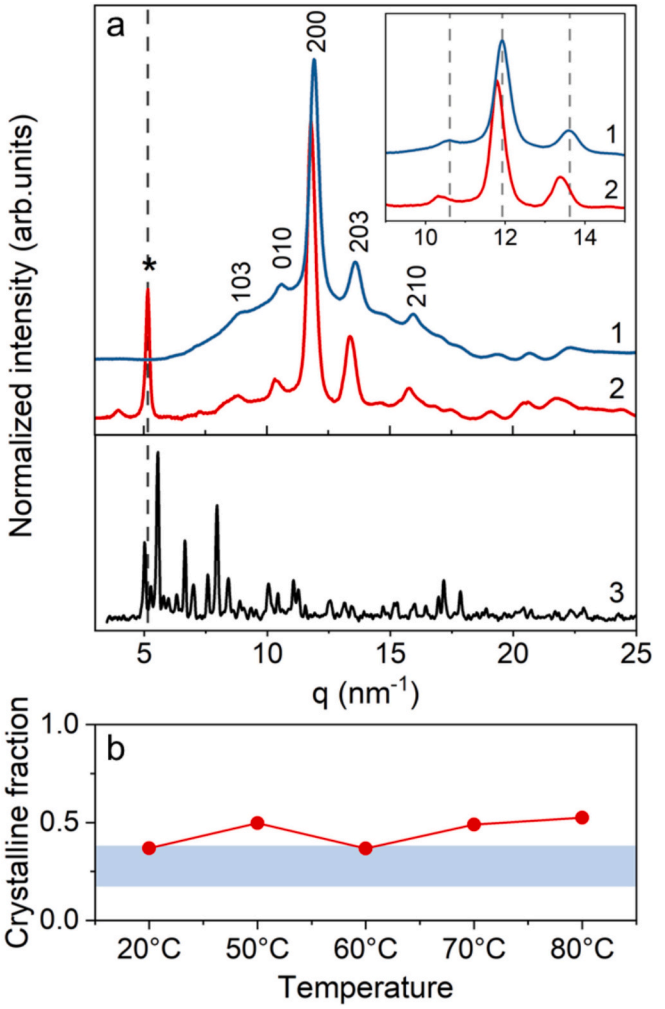

Fig. 4. Eu-incorporation structural effects. (a) Top: GIXD patterns of PLLA and Eu-modified PLLA microsphere samples (curve 1 in blue and curve 2 in red, respectively) prepared at 20 °C. The asterisk indicates the additional feature in Eu-PLLA. Inset: amplified view with dashed lines highlighting the shift of the main reflections. Curve 3: XRD pattern of $Eu(acac)_3$. (b) Crystalline fraction – from the area of the amorphous halo at q vectors between 7 and 18 nm^{-1} and the integrated pattern – in samples obtained at different temperature. The shadowed region shows the range of values observed in Eu-free samples [15]. (For interpretation of the references to color in this figure legend, the reader is referred to the web version of this article.)

survives after heating at 180 °C and is also observed by cooling, while the diffraction peaks of PLLA disappear above T_m and appear again by cooling from melt. These outcomes exclude the occurrence of segregated $Eu(acac)_3$ and suggest that the 5 nm^{-1} diffraction peak is due to ordered domains of different types, which are thermally more stable than $Eu(acac)_3$ and even more stable than Eu-free PLLA. Some more details of the ordered structure responsible for the diffraction peak at 5 nm^{-1} will be given in Section 3.8.

3.4. Spatial distribution of Eu-modified domains

From GIXD data it clearly resulted that an Eu-rich region is present in the Eu-modified PLLA microspheres. It was therefore necessary to investigate where it was actually located, whether inside the microspheres or forming an Eu-rich shell outside them. The first evidence comes from SEM analyses of microsphere sections (Fig. 7a), where whitish regions can be found dispersed inside the PLLA matrix, possibly attributed to Eu aggregations. Since SEM is rather surface sensitive, the exact location of these aggregates cannot be exactly determined. μCT imaging from diluted microsphere dispersions (Fig. 7b) give an interesting information on the micro-morphology of the Eu distribution, as shown by the yellowish bright regions located within the microspheres. Further images from both techniques collected from both Eu-free and Eu-modified microspheres are presented in Figs. S4 and S5 in SI. The images indeed provide evidence of regions with a significantly higher density within the compact polymer matrix, caused by efficient electron scattering in SEM, or X-ray absorption in μCT images, respectively. Thus, it was clearly shown the occurrence of Eu-rich regions distributed inside the microspheres and surrounded by an Eu-poor PLLA matrix. These regions are found in the interior of the microspheres, not on the surface or in the inner core. From the μCT scanning, the high-density regions appear indeed clearly placed below the surface in all the microspheres of the analysed ensemble.

This result raises the question of how europium is incorporated into these regions. In the next sections the photoluminescence spectroscopy of incorporated Eu^{3+} ions and the analysis of the phonon spectrum of the Eu-modified microspheres shed some light on the possible structures and

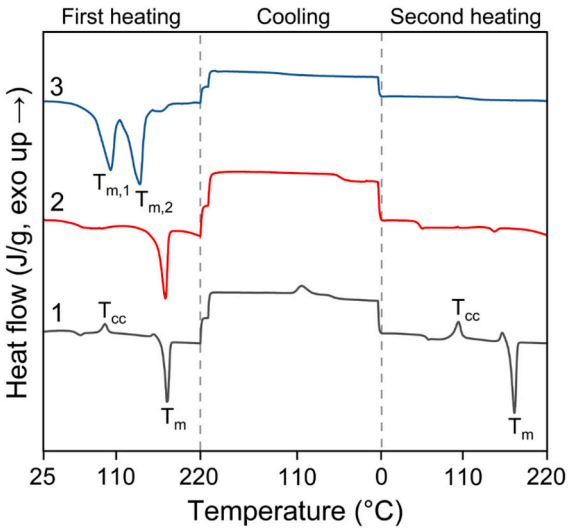

Fig. 5. Eu effects on crystallization of PLLA microspheres. DSC curves along heating ramp from 25 to 220 °C, followed by cooling at 0 °C and second heating at 220 °C of Eu-free (curve 1 in black) and Eu-modified (curve 2 in red) PLLA microspheres both prepared at 20 °C, compared with $Eu(acac)_3$ (curve 3 in blue). Cold crystallization (T_{cc}) and melting (T_m) temperatures are indicated on curves 1 and 2. The two melting temperatures for $Eu(acac)_3$ ($T_{m,1}$ and $T_{m,2}$) are indicated for curve 3. (For interpretation of the references to color in this figure legend, the reader is referred to the web version of this article.)

environment generated by the presence of Eu ions.

3.5. A spectroscopic view on Eu-incorporation in PLLA microspheres

The PL spectrum of the f-f transitions of Eu^{3+} ions is a probe of the direct surrounding of europium, providing some details on the first coordination shell, and revealing changes with respect to the parent molecular cage in $Eu(acac)_3$. Fig. 8 reports the PL spectrum of the first three transitions $^5D_0 \rightarrow {}^7F_J$ excited at 488 nm (with j = 0, 1, and 2) in $Eu(acac)_3$ (Fig. 8a) and a representative sample of Eu-modified PLLA microspheres (Fig. 8b).

There are differences both in the relative intensity and in the shape of the emissions, indicating that substantial changes occur in symmetry and intensity of the electrostatic field arising from the first coordination shell of the Eu^{3+} central ion. In this analysis, the emission band at about 595 nm, arising from the magnetic dipole transition $^5D_0 \rightarrow {}^7F_1$, can be taken as an intensity reference, since its integrated intensity is largely insensitive to the electrostatic field of the ligands [21,22]. The narrow peak at about 580 nm, arising from the non-degenerate $^5D_0 \rightarrow {}^7F_0$ transition, is strictly forbidden by the standard selection rule on ΔJ, and is indeed lacking in high symmetry complexes. Its detection here – with intensity comparable to or exceeding that of the $^5D_0 \rightarrow {}^7F_1$ transition – is an indication of a quite low symmetry of the Eu^{3+} environment, able to cause a not negligible *J*-mixing within the $4f^6$ configuration [22]. Additionally, the splitting of the $^5D_0 \rightarrow {}^7F_0$ peak, if present (as in the spectrum of $Eu(acac)_3$), cannot be ascribed to split levels (which are indeed not-degenerate), but rather to different sites in the system. The third band at about 615 nm is the most intense one. It arises from the $^5D_0 \rightarrow {}^7F_2$ transition, whose integrated intensity and shape are strongly influenced by symmetry and intensity of the ligand field [21].

The comparison between the PL spectrum of Eu^{3+} in PLLA microspheres and that of $Eu(acac)_3$ in Fig. 8 shows relevant deviations both in the relative intensities of the emissions and even in the shape of each detected band. Such a result suggests that the lanthanide ions find a distinct coordination in the PLLA matrix, potentially regarding several features, such as local symmetry, coordination number, and mean ligand distance. Variability in the shape and the relative intensity are also registered comparing PL spectra of different microspheres (inset in Fig. 8b). However, the spectra of different microspheres are much more similar to each other than to $Eu(acac)_3$ spectrum, which also displays some variability from site to site, as shown in inset of Fig. 8a.

Fig. 9 reports the results of the quantitative and statistical analysis of the main spectral features registered within one of the microsphere batches, compared with the results collected in $Eu(acac)_3$. The figure reports the normalized integrated intensities of the $^5D_0 \rightarrow {}^7F_0$ and $^5D_0 \rightarrow {}^7F_2$ transitions with respect to the $^5D_0 \rightarrow {}^7F_1$ transition as a reference.

The comparison between relative intensities supports the presence of clear-cut differences between Eu sites in PLLA microspheres and those in $Eu(acac)_3$, more relevant than the variations from site to site within the polymeric matrix of PLLA microspheres (quantified by the error bars in Fig. 9). The abovementioned spectroscopic results provide some hints on the coordination of europium in PLLA microspheres, using $Eu(acac)_3$ as a reference. Smaller values of relative integrated intensity of both the $^5D_0 \rightarrow {}^7F_0$ and $^5D_0 \rightarrow {}^7F_2$ transitions in Eu-modified PLLA with respect to $Eu(acac)_3$ (Fig. 9) suggest that the local ligand field is less effective in *J*-mixing. Therefore, the Eu^{3+} sites in PLLA microspheres result to be

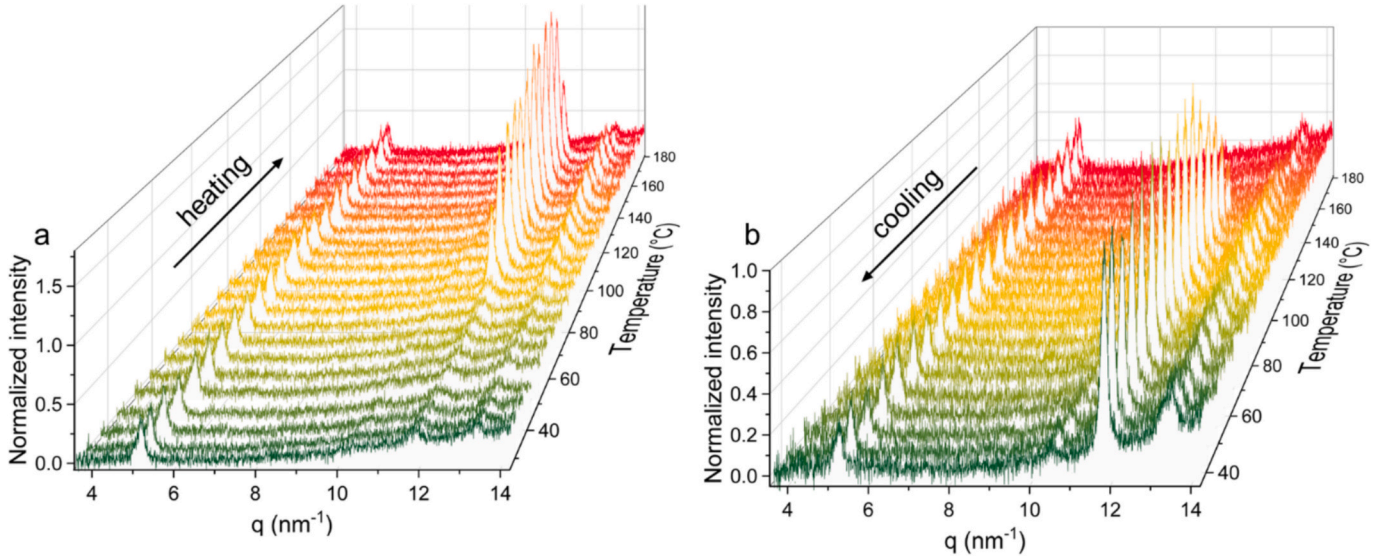

Fig. 6. Temperature dependence of the Eu-modified PLLA structure. PXRD patterns of Eu-modified PLLA microspheres, prepared at 20 °C, collected at different temperature (a) by heating from room temperature to 180 °C and (b) by cooling from 180 °C, at step of 10 °C.

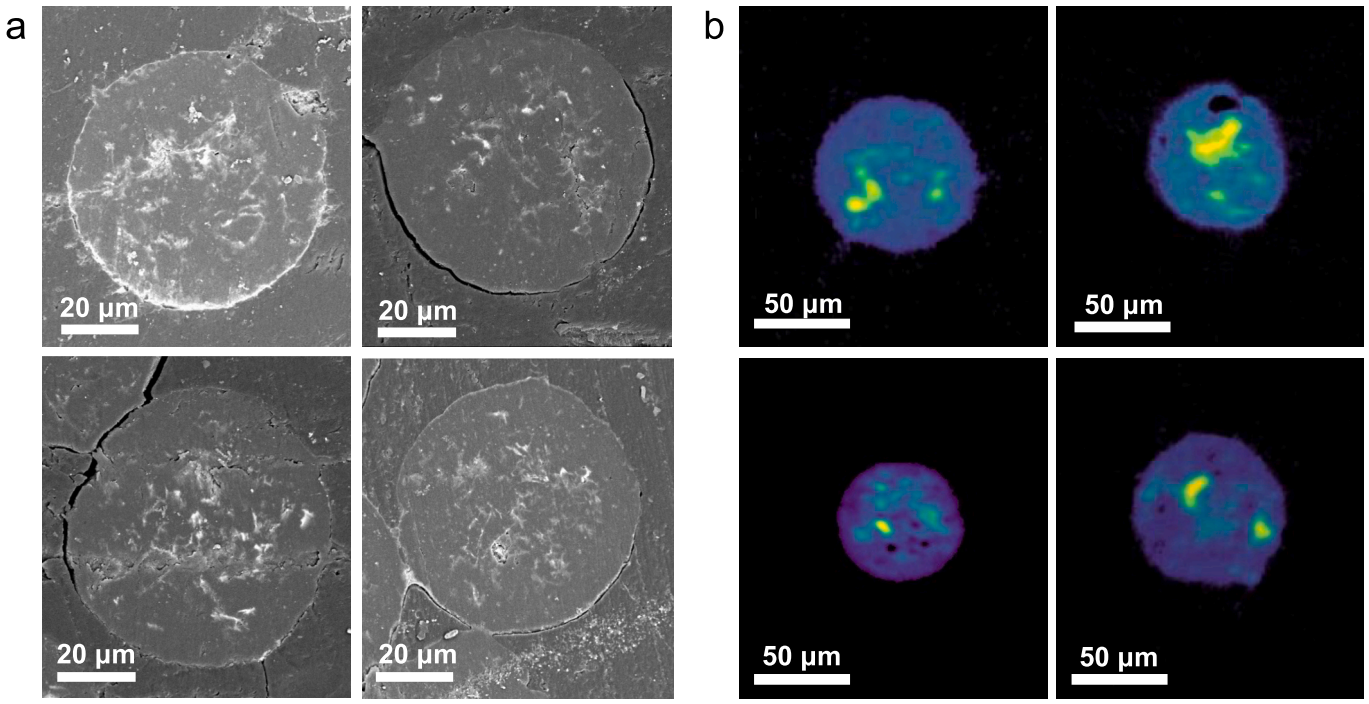

Fig. 7. Inner view of Eu-modified PLLA microspheres. (a) SEM and (b) μCT images of representative sections of Eu-modified PLLA microspheres.

characterized by higher symmetry and/or weaker ligand field intensity –the latter one caused by either a slight increase of the mean Eu—O distance or a lowering of the mean number of ligands. One of the main sources of asymmetry in the ligand field around Eu^{3+} in $Eu(acac)_3$ is the presence of two water molecules in its eight-fold coordination shell [23]. The substitution of water molecules by carboxyl groups in the Eu^{3+} coordination shell in the PLLA matrix would therefore be consistent with an increase of local symmetry and a resulting decrease of *J*-mixing, as suggested by the data in Fig. 9. On the other hand, a lower intensity of the ligand field in PLLA than in $Eu(acac)_3$ could also reasonably arise from slightly larger Eu—O mean distance, since the mean distance between carboxyl groups in PLLA chains is larger than in $Eu(acac)_3$ (0.293 nm from data in [24] and 0.278 nm from data in [23], respectively). In the next section, Raman and IR data give additional clues of the Eu^{3+} coordination in PLLA microspheres, evidencing molecular structures similar but distinct from $Eu(acac)_3$ resulting from the Eu incorporation in the polymer matrix.

3.6. *Eu-perturbation of the PLLA phonon spectrum*

The Raman spectrum of Eu-modified PLLA microspheres shows some peculiarities with respect to pure PLLA. The analysis of these anomalies can provide information on how Eu is structurally incorporated inside the microspheres.

Curve 1 in Fig. 10 reports the Raman spectrum of a pure PLLA microsphere, as a reference, in the spectral range 200–1800 cm^{-1}. All the detected modes correspond to the modes expected in PLLA [25]. In the same figure, curves 2 and 3 are the single-particle Raman spectra of two Eu-modified microspheres, representative of two limit situations of microspheres with low (curve 2) and high (curve 3) europium content, giving rise to spectral modifications with respect to pure PLLA. The most evident differences consist of vibrational modes that do not belong to the vibrational spectrum of PLLA and fall in spectral positions matching, to some extent, some vibrational modes that are detected in the $Eu(acac)_3$ Raman spectrum (curve 4) [26].

A structured weak feature is also observed in the range 1500–1600 cm^{-1} from weak photoluminescence arising from the Eu^{3+} transition $^5D_0 \rightarrow {}^7F_4$ excited – with a very small efficiency – by the Raman spectrometer laser at 633 nm. This attribution is indeed confirmed by the observation of the same emissions (reported in Fig. S6 in SI) when excited at 488 nm on the same microspheres of curves 2 and 3 in Fig. 10 in the same conditions. Importantly, looking at Fig. 10, the additional phonon modes in the Raman spectra – those not belonging to the phonon spectrum of Eu-free PLLA – are more intense in the microsphere with higher intensity of the Eu^{3+} emission at 1500–1600 cm^{-1}. This result – confirmed by the analysis of multiple microspheres in all the investigated batches – brings to ascribe these modes to molecular groups strictly related to the incorporation of Eu^{3+} ions in the microspheres.

The comparison with the $Eu(acac)_3$ Raman spectrum suggests that the additional modes in Eu-modified PLLA microspheres arise from three main types of groups, according to the interpretation of analogous spectral features in the $Eu(acac)_3$ Raman spectrum [27]. The first kind of these groups includes Eu—O units and chelating C═O groups, with stretching modes potentially responsible for the spectral contributions at 411 and 921 cm^{-1}. Second types of structures are CH_3 groups with their in-plane and out-of-plane deformation modes, corresponding to the peaks detected at 570, 1273, and 1369 cm^{-1}. Finally, $Eu<^{O=C}_{O=C}\rangle$ coordination rings appear to be involved, as in $Eu(acac)_3$, with a deformation mode potentially responsible for the peak at 668 cm^{-1}, with a possible contribution from C—CH_3 stretching.

It is worth noting that, despite the general agreement between the additional modes and the $Eu(acac)_3$ spectrum, some of these modes however show a non-negligible shift with respect to $Eu(acac)_3$ modes (namely the modes at 668 and 1273 cm^{-1}, shifted by approximately 8 cm^{-1}), while others are almost lacking (specifically, the $Eu(acac)_3$ modes at 1020 and 1193 cm^{-1}). These discrepancies suggest that the Eu incorporation in emulsified microspheres does not proceed as an additive incorporation of $Eu(acac)_3$ molecular units or even larger segregated $Eu(acac)_3$ domains in the polymeric matrix. Rather, some change in the Eu^{3+} coordination occurs with respect to $Eu(acac)_3$, as also indicated by PL spectroscopy (Figs. 8 and 9). Interaction with PLLA chains likely takes place when Eu^{3+} ions enter the forming microspheres.

This result is indeed suggested by experimental clues regarding the almost full removal of detectable vibrational fingerprints of alkene CH groups (olefinic CH), a distinctive component of $Eu(acac)_3$ molecule

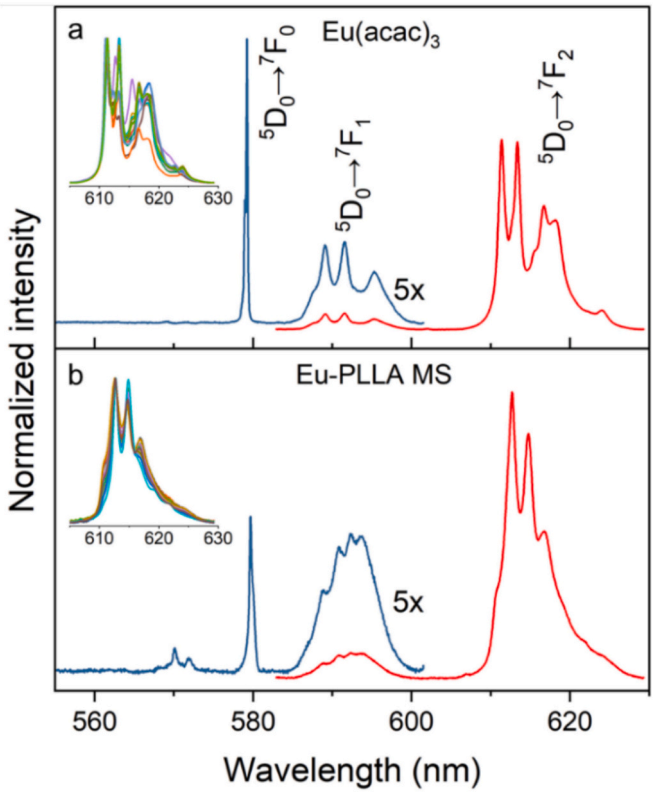

Fig. 8. PL spectra of Eu^{3+} ions incorporated in PLLA microspheres. 488 nm excited PL spectrum of Eu^{3+} ions in the range 555–630 nm in (a) a powder sample of $Eu(acac)_3$, and (b) a representative Eu-modified PLLA microsphere sample synthesized at 20 °C. Insets: envelope of spectra collected in similar conditions from (a) different points of the sample, and (b) different microspheres of the same batch. The responsible transitions of Eu^{3+} ions are indicated. The blue spectra are enlarged by a factor 5 to better see the transitions, since their intensity is much lower than the ones in red spectra. (For interpretation of the references to color in this figure legend, the reader is referred to the web version of this article.)

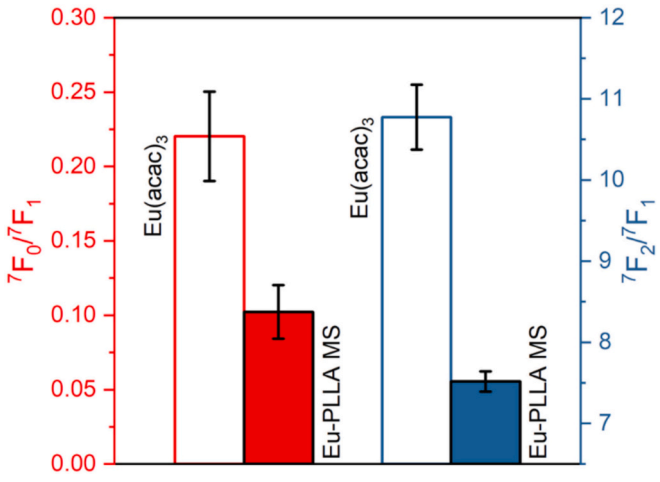

Fig. 9. Intensity of Eu^{3+} PL bands. Integrated intensity of the PL $^5D_0 \rightarrow {}^7F_0$ and $^5D_0 \rightarrow {}^7F_2$ transitions (axis on the left and on the right, respectively) with respect to the $^5D_0 \rightarrow {}^7F_1$ transition of Eu^{3+} ions in Eu-modified PLLA microspheres synthesized at 20 °C (filled bars) and in $Eu(acac)_3$ (empty bars).

with respect to PLLA. For instance, the narrow peak at 1193 cm^{-1} in the $Eu(acac)_3$ Raman spectrum (curve 4 in Fig. 10), which is a complex mode with a contribution from olefinic CH bending mode [27,28], is missing in the Eu-modified microspheres. The lack of alkene CH groups of $Eu(acac)_3$ molecules is also supported by the FTIR spectrum of Eu-modified PLLA microspheres (curve 1 in Fig. 11), in which there is no detectable evidence of the olefinic CH stretching mode at 3075 cm^{-1} [27,28] observed in $Eu(acac)_3$ (curve 2 in Fig. 11). The FTIR spectra in Fig. 11 register a further experimental indication that Eu incorporation in PLLA microspheres does not proceed by $Eu(acac)_3$ embedding. In fact, the region at around 2900–3000 cm^{-1} – from ethyl and methyl stretching modes – is quite different from $Eu(acac)_3$, especially lacking the stretching mode of CH_3 groups in $Eu(acac)_3$ at 2925 cm^{-1}.

3.7. The role of PLLA chains in the Eu^{3+} coordination shell

All the spectroscopic results – from PL, Raman, and FTIR spectra – converge towards a common conclusion: Eu^{3+} ions enter PLLA microspheres creating a coordination that is distinct from that of Eu^{3+} in the precursor molecular compound. As a matter of fact, from the analysis of PL spectra, the coordination shell results to possess lower asymmetry and/or weaker ligand field compared to $Eu(acac)_3$. Furthermore, FTIR spectroscopy shows the absence of important vibrational fingerprints of $Eu(acac)_3$ molecule in the microspheres, thus excluding a direct embedding of entire precursor molecules, as well as larger segregated domains of precursor compound. Nevertheless, the incorporation of Eu^{3+} ions into PLLA is accompanied by additional molecular groups, as evidenced by additional vibrational modes in the Raman spectrum that are quite similar to those associated with the Eu coordination in $Eu(acac)_3$.

Notably, the molecular groups responsible for these modes are potentially compatible both with the molecular structure of perturbed (acac) fragments and some features of PLLA chains. Both systems can indeed accommodate bonds with Eu^{3+} ions through C═O chelating groups, forming rings connected to a backbone which comprises CH_3 groups. Therefore, while the direct embedding of unperturbed $Eu(acac)_3$ molecules can be excluded, the spectroscopic results are compatible with the formation of Eu^{3+} coordination shells involving interactions with modified (acac) groups and/or chelating groups along the PLLA chains. The formation of this kind of coordination by interaction between ion complexes and different molecular chains is indeed observed in many other systems [1–5], including polymers prepared with $Eu(acac)_3$ [29,30].

In the present case, the interaction between Eu^{3+} and PLLA chains can be the result of two main factors. The first one is the property of PLLA as chelating agent through its carboxylic groups. PLLA is rarely exploited as chelating agent because much more effective chelating molecules usually give much better results in several areas. Chelating action is however present in PLLA and even used in some cases, for instance in the field of food and agriculture where PLLA can play a role as natural chelating agent of metal elements in mineral components [31]. Second factor is the different acid dissociation constant of acetylacetone with respect to PLLA, with pK_a values of about 9 [32] and 4 [33], respectively. This fact makes it likely for Eu^{3+} ions to form coordination bonds with PLLA chains during microsphere formation by emulsification, since the process involves PLLA chains and $Eu(acac)_3$ molecules fully dissolved in the starting organic solution and ready to interact one-to-one in the water solution during the emulsification. During emulsification, the cage of (acac) molecules can thus be dismissed by Eu^{3+} ions, at least partially, for new bonds with PLLA carboxyl groups.

3.8. Effects of Eu-PLLA coordination on the polymer structure

Based on the above spectroscopic results and XRD data, it follows that Eu^{3+} ions in PLLA can create coordination shells that involve not only (acac) molecules but also carboxyl groups along the PLLA chains. Accordingly, Eu^{3+} ions can work as bridges between two or more PLLA chains in quite stable structures, forming sequences of heavy ions with a

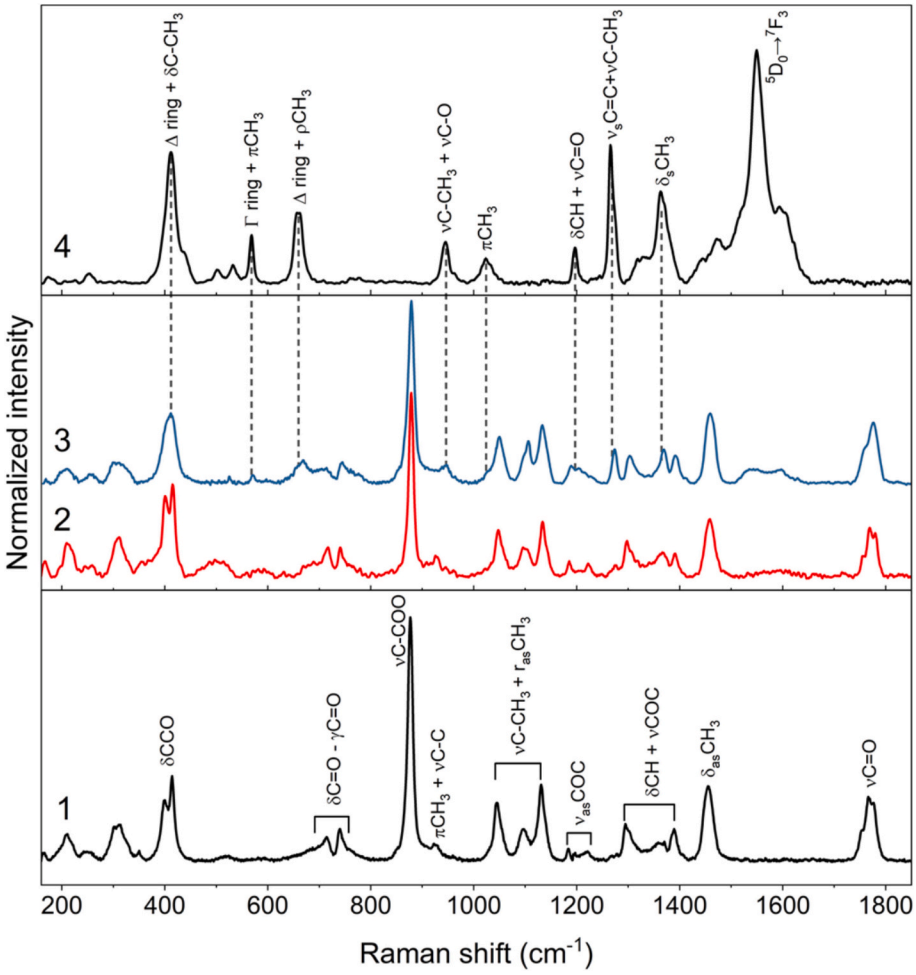

Fig. 10. Raman modes in Eu-modified PLLA microspheres. Raman spectra of Eu-free PLLA microsphere (curve 1) and Eu-modified PLLA microspheres with low and high Eu content (curves 2 and 3, respectively) as qualitatively monitored by the intensity of the Eu^{3+} transition $^5D_0 \rightarrow {}^7F_4$ transition excited at 633 nm and falling in an apparent Raman shift position of about 1600 cm^{-1}. Dashed vertical lines indicate the position of the main phonon modes in the spectrum of $Eu(acac)_3$ (curve 4). Assignments to vibrational modes of molecular groups in PLLA and in $Eu(acac)_3$ are reported with curves 1 and 4.

periodicity regulated by the sequence of carboxyl groups along the PLLA chain, similarly to structures in other rare-earth -containing polymers [1,2,5]. This view is indeed confirmed by the effects of Eu incorporation on the XRD patterns in Fig. 4a. Both the isolated diffraction peak at about 5 nm^{-1} and the shift of the main PLLA diffraction peaks at about 12 and 14 nm^{-1} (200 and 203 reflections, respectively) towards smaller values are indeed consistent with intercalated sequences of Eu bridges between the chains, which slightly enlarge the unit cell, mainly in the (100) direction.

Importantly, the dissolution of the $Eu(acac)_3$ molecules with the formation of O-Eu-O bridges substituting for interchain hydrogen bonds also explain further peculiarities of Eu-modified PLLA microspheres highlighted by temperature-dependent XRD measurements and DSC data. Specifically, looking at the data in Fig. 6, the single small-angle XRD reflection at about 5 nm^{-1} reveals the presence of domains with a low-dimensional chain-like periodicity – which show a thermal stability higher than the PLLA matrix. Such a result is consistent with the formation of structures of few PLLA chains which are held together by O-Eu-O bridges belonging to Eu coordination shells and substituting for the less thermally stable inter-chain hydrogen bonds of pure PLLA. Furthermore, the presence of aligned PLLA chains stabilized by Eu coordination shells can also work as crystallization agents, promoting higher crystallinity within the microspheres by emulsification, and crystallization from melt, in agreement with the experimental data in Figs. 4b and 6.

3.9. Role of Eu incorporation on the structural stability

The structural stability of Eu-modified PLLA microspheres is responsible, to some extent, of the results in Fig. 2 and Fig. 3b regarding the morphological microsphere stability and the good retention of lanthanide ions after prolonged stay in buffer solution. This aspect can further be analysed by spectroscopy monitoring the changes in Eu^{3+} PL parameters along the time of stay in buffer solution.

The results are presented in Fig. 12, also comparing data from microsphere batches prepared at different emulsification temperature. Most of the registered variations vs. degradation time does not exceed the statistical uncertainty arising from the dispersion of values within each sample, regarding the relative integrated intensity. However, in some cases, the data reveals that the relative integrated intensity of the $^5D_0 \rightarrow {}^7F_2$ and $^5D_0 \rightarrow {}^7F_0$ transitions show reliable evidence of some changes in the first steps of the treatment in buffer solution, without further relevant effects by prolonged stay. Interestingly, the microsphere batches which show this initial lowering of intensity are those prepared at temperature comparable or higher than the glass transition temperature (T_{emu} ranging from 60 to 80 °C). The effect is not however accompanied by significant changes of bandwidth of the $^5D_0 \rightarrow {}^7F_2$ emission (Fig. 12).

The initial change of relative emission intensity points to a change of branching ratio between the different radiative decay channels of Eu^{3+} ions. This fact implies changes in the symmetry and/or polarizability in

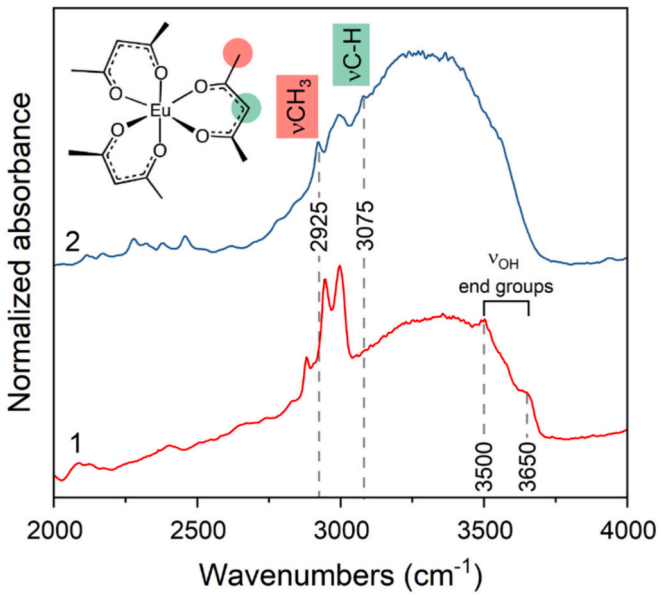

Fig. 11. FTIR spectra of Eu-modified PLLA microspheres and $Eu(acac)_3$. Infrared absorption spectra in the region of C—H and O—H stretching modes of Eu-modified PLLA microspheres (curve 1 in red) and $Eu(acac)_3$ (curve 2 in blue). Dashed lines at 2925 and 3075 cm^{-1} indicate the modes of specific groups in the $Eu(acac)_3$ molecular structure (highlighted in the scheme in inset). (For interpretation of the references to color in this figure legend, the reader is referred to the web version of this article.)

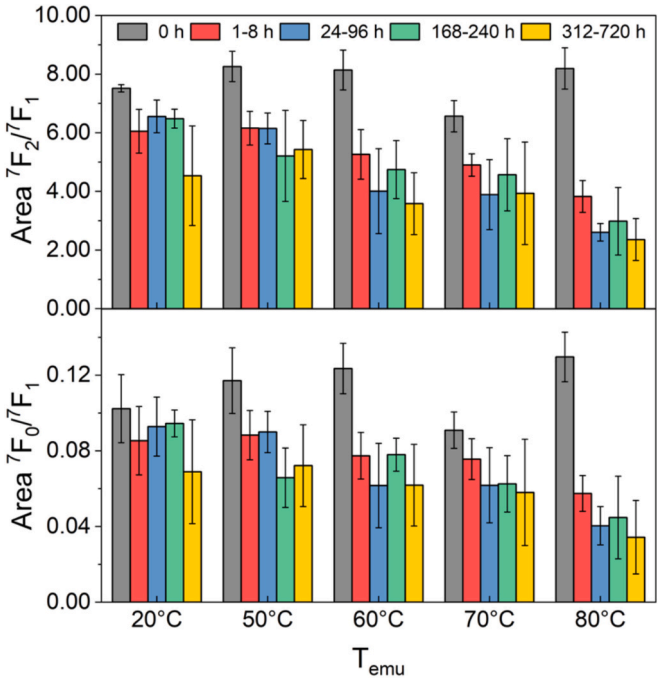

Fig. 12. Degradation of PL features. Integrated intensity of the $^5D_0 \rightarrow {}^7F_0$ and $^5D_0 \rightarrow {}^7F_2$ transitions normalized by the $^5D_0 \rightarrow {}^7F_1$ transition of Eu^{3+} ions in PLLA microspheres prepared at different emulsification temperature and degradation time in buffer solution.

the environment of the Eu^{3+} ions [22]. Such changes can result from structural modifications caused by adsorption of water molecules during the stay in buffer solution. This process can in fact change the relative intensity of the emission bands, besides, to some extent, the overall emitted intensity through the activation of non-radiative decay [34,35].

Adsorption and diffusion of water molecules can indeed take place in PLLA [36] despite its hydrophobic nature, with also a role of surface morphology and porosity. As a matter of fact, evidence of a slightly higher surface porosity in microspheres emulsified at high temperature comes from SEM images (Fig. S2).

Confirmation of traces of hydration can be found in the FTIR spectrum. Curves 1 and 2 in Fig. 13a reports FTIR spectra of a sample prepared at 60 °C before and after treatment in buffer solution, respectively, in the region of the stretching modes of water molecules at around 3300 cm^{-1}.

The broad band from water molecules – centred at about 3300 cm^{-1} – is more pronounced after the treatment, compared with the other features of the phonon spectrum, supporting the embedding of H_2O into the microspheres and the possible modification of the environment of Eu^{3+} sites. Unexpectedly, such modification does not sensibly affect the broadening of the $^5D_0 \rightarrow {}^7F_2$ emission (Fig. 12). Nevertheless, some effects can be highlighted looking at the shape of the emission band. The inset of Fig. 13a reports two PL spectra – collected before and after

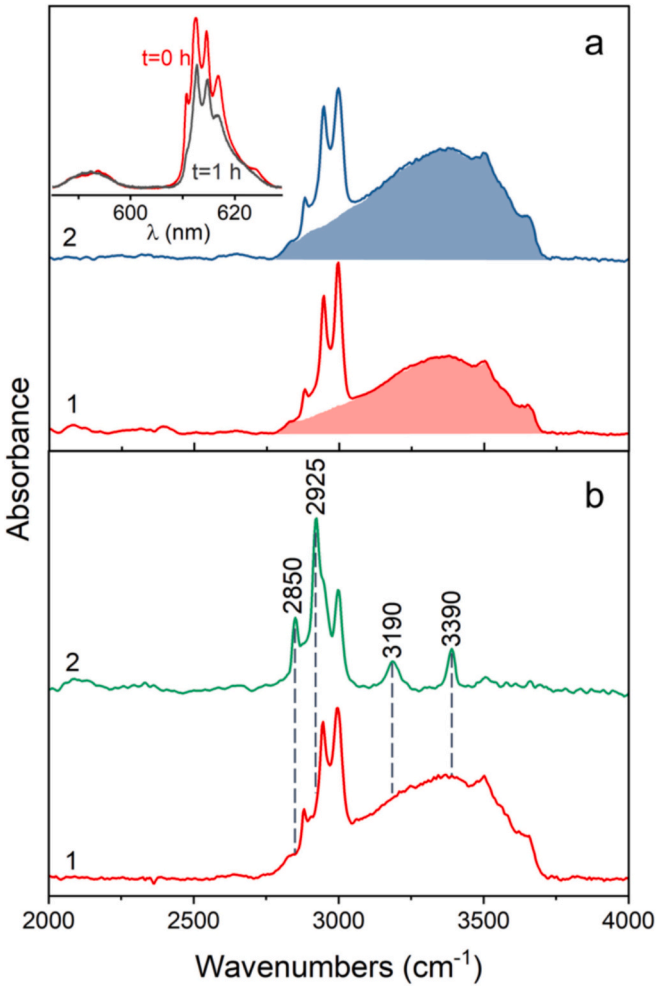

Fig. 13. Degradation and irradiation effects. (a) Infrared absorption spectra, in the C—H and O—H stretching region, of Eu-modified PLLA microspheres prepared at 60 °C, before (curve 1) and after (curve 2) degradation in buffer solution for 1 month (shaded regions correspond to the water OH stretching band). Inset: PL spectra recorded before and after 1 h of degradation in buffer solution. (b) Infrared spectrum of Eu-modified PLLA microspheres prepared at 60 °C after exposure to an X-ray dose of 100 Gy (curve 1 in red) compared to the spectrum of a PLLA bulk sample exposed to the same dose (curve 2 in green), in which the effects of radiation-induced degradation are present (labels on curve 2). (For interpretation of the references to color in this figure legend, the reader is referred to the web version of this article.)

treatment in buffer solution for 1 h – showing a detectable spectral redistribution of the light emission intensity. Importantly, such effects appear relevant only in samples prepared at 60, 70 and 80 °C (Fig. S7). These results confirm, on the one hand, that more pronounced changes occur in the ligand field when the sample shows a small but significant lowering of PL intensity after treatment in buffer solution. On the other hand, the results also show that the effects on the Eu^{3+} environment do not proceed after the first hour of treatment. The compact morphology of the microspheres, displayed in the SEM images (Fig. 7a), can strongly hinder the embedding of water molecules and be partially responsible for the stability of the structure against the hydration process. Furthermore, no trace of Eu^{3+} PL has been detected in the buffer solution after treatment and, specifically, of water coordinated Eu^{3+} ions whose PL spectrum is known to be characterized by a very weak $^5D_0 \rightarrow {}^7F_0$ peak and a significantly lower intensity of the $^5D_0 \rightarrow {}^7F_2$ band compared to the $^5D_0 \rightarrow {}^7F_1$ band [37,38].

Fig. 13b also reports the infrared spectrum of a sample of the same batch (by emulsification at 60 °C) after exposure to an X-ray irradiation test dose of 100 Gy (curve 1) to observe the possible onset of radiation induced molecular damage within the PLLA structure of the microspheres. The spectrum does not show any relevant change of molecular modification compared to a reference PLLA sample in which the effects of the radiation-induced mechanism are clearly visible (curve 2) [14]. Namely, there is no evidence of modes at 2850 and 2925 cm^{-1} from transformation of methyl groups to CH_2 groups, and at 3180 and 3390 cm^{-1} from OH groups formed by hydroxylation of carbonyl group [14].

4. Conclusions

The rich collection of complementary data – coming from microscopy, tomography, diffractometry, calorimetry, and spectroscopy – gives valuable insights into the mechanisms responsible for europium incorporation in PLLA microspheres by emulsification. Eu^{3+} ions are demonstrated to enter PLLA microsphere forming a coordination shell distinct from that of $Eu(acac)_3$ (see PL data), interacting with the polymer chains and coordinating with PLLA carboxyl groups (see Raman and IR data). The Eu incorporation in PLLA microspheres by emulsification gives rise to microspheres with a higher crystallinity with respect to pure PLLA microspheres (see XRD data), but with an amorphous polymer fraction which shows a reduced capacity of crystallization (see DSC data), while maintaining compact micro-morphology (see SEM analysis). The involvement of PLLA chains into the Eu^{3+} coordination shell generates thermally stable ordered domains of Eu-rich regions in the inner part of the microspheres (temperature variable XRD and μCT analysis). Finally, the interaction between lanthanide ions and polymer can be varied by changing the emulsification temperature (see PL data), allowing the tuning of the level of matrix reinforcement against too rapid degradation and damage, and the possible ion release (see XRF, PL and IR data after treatment in buffer solution and irradiation), forming a reliable basis for designing the system for applications. Our study indeed demonstrates that the effects of emulsification temperature on PLA structure, Eu incorporation, and Eu release during degradation can be used as an unprecedented tool for regulating the material properties of polymer microspheres. Furthermore, the data on the Eu-induced inhibition of PLLA crystallization can also provide a tool for the modulation of PLLA crystallization potentially useful in a wide range of applications. Notably, this strategy circumvents the need for additives, which, although widely used in other fields, may alter the biocompatibility of the material and introduce potential risks in medical applications.

CRediT authorship contribution statement

Giulia Tamburini: Writing – review & editing, Visualization, Investigation, Formal analysis, Conceptualization. **Fabian Gasser:** Investigation. **Eduardo Machado Charry:** Investigation. **Roland Resel:** Supervision, Investigation. **Giulia Tarricone:** Investigation. **Sergio Piva:** Investigation. **Adele Sassella:** Conceptualization. **Roberto Lorenzi:** Writing – review & editing, Supervision, Methodology. **Alberto Paleari:** Writing – original draft, Project administration, Methodology.

Declaration of competing interest

The authors declare the following financial interests/personal relationships which may be considered as potential competing interests: Giulia Tamburini reports financial support was provided by Galatea Bio Tech S.r.l. and the Ministry of the Research and University. If there are other authors, they declare that they have no known competing financial interests or personal relationships that could have appeared to influence the work reported in this paper.

Acknowledgements

G.T. gratefully acknowledges the financial support from Galatea Bio Tech S.r.l. and the Ministry of the Research and University (Project FSE REACT-EU, IV.5 Action, DM 1061/2021). The authors also thank Prof. Paola Branduardi, Chief Scientific Officer of Galatea Bio Tech S.r.l., for useful discussions. Special thanks to Elettra Sincrotrone Trieste for providing access to the SAXS beamline (proposal 20232068), and Sumea Klokic and Philipp Aldo Wieser for their assistance.

Appendix A. Supplementary data

Supplementary data to this article can be found online at https://doi.org/10.1016/j.reactfunctpolym.2025.106382.

Data availability

Data will be made available on request.

References

[1] T. Nakanishi, J. Xu, N. Hirosaki, T. Takeda, Thermostable europium polymer crystalline spherical beads and their photophysical properties, Sensors Mater. 35 (2) (2023) 529–536, https://doi.org/10.18494/SAM4150.
[2] A. Nakajima, T. Nakanishi, Y. Kitagawa, T. Seki, H. Ito, K. Fushimi, Y. Hasegawa, Hyper-stable organo-Eu^{III} luminophore under high temperature for photo-industrial application, Sci. Rep. 6 (2016) 24458, https://doi.org/10.1038/srep24458.
[3] O. Essahili, A. El Azzaoui, M. Ilsouk, O. Moudam, Investigating the long-term stability of photoluminescence lifetimes in PMMA films doped with β-diketonate europium complexes based on bipyridine and terpyridine derivatives, J. Photochem. Photobiol. A Chem. 447 (2024) 115211, https://doi.org/10.1016/j.jphotochem.2023.115211.
[4] T.A. Kovacs, M.C.F.C. Felinto, T.B. Paolini, B. Ali, L.K.O. Nakamura, E.E. S. Teotonio, H.F. Brito, O.L. Malta, Synthesis and photoluminescence properties of [Eu(dbm)3·PX] and [Eu (acac)3·PX] complexes, J. Lumin. 193 (2018) 98–105, https://doi.org/10.1016/j.jlumin.2017.09.029.
[5] Y. Hasegawa, Y. Kitagawa, Luminescent lanthanide coordination polymers with transformative energy transfer processes for physical and chemical sensing applications, J. Photochem. Photobiol. C Photochem. Rev. 51 (2022) 100485, https://doi.org/10.1016/j.jphotochemrev.2022.100485.
[6] A. Nakajima, T. Nakanishi, Y. Kitagawa, K. Fushimi, Y. Hasegawa, Thermosensitive luminescent lanthanide complex with two photosensitized ligands, Sensors Mater. 28 (8) (2016) 845–850.
[7] K. Yavari, E. Yeganeh, H. Abolghasemi, Production and characterization of ^{166}Ho polylactic acid microspheres, J. Label. Compd. Radiopharm. 59 (2016) 24–29, https://doi.org/10.1002/jlcr.3366.
[8] R.C. Bakker, R. de Roos, F.F. Tessa Ververs, M.G.E.H. Lam, M.K. van der Lee, B. A. Zonnenberg, G.C. Krijger, Blood and urine analyses after radioembolization of liver malignancies with [^{166}Ho]Ho-acetylacetonate-poly(L-lactic acid) microspheres, Nucl. Med. Biol. 71 (2019) 11–18, https://doi.org/10.1016/j.nucmedbio.2019.03.001.
[9] J.F.W. Nijsen, M.J. van Steenbergen, H. Kooijman, H. Talsma, L.M.J. Kroon-Batenburg, M. van de Weert, P.P. van Rijk, A. de Witte, A.D. van het Schip, W. E. Hennink, Characterization of poly(L-lactic acid) microspheres loaded with holmium acetylacetonate, Biomaterials 22 (2001) 3073–3081, https://doi.org/10.1016/S0142-9612(01)00055-2.
[10] Y.-H. Wong, H.-Y. Tan, A. Kasbollah, B.J.J. Abdullah, R. Udyavara Acharya, C.-H. Yeong, Neutron-activated biodegradable samarium-153 acetylacetonate- poly-L-lactic acid microspheres for intraarterial radioembolization of hepatic tumors.

World, J. Exp. Med. 10 (2) (2020 March 30) 10–25, https://doi.org/10.5493/wjem.v10.i2.10.
[11] F. Ramazani, W. Chen, C.F. van Nostrum, G. Storm, F. Kiessling, T. Lammers, W. E. Hennink, R.J. Kok, Strategies for encapsulation of small hydrophilic and amphiphilic drugs in PLGA microspheres: state-of-the-art and challenges, Int. J. Pharm. 499 (2016) 358–367, https://doi.org/10.1016/j.ijpharm.2016.01.020.
[12] Y. Hua, Y. Su, H. Zhang, N. Liu, Z. Wang, X. Gao, J. Gao, A. Zheng, Poly(lactic-co-glycolic acid) microsphere production based on quality by design: a review, Drug Deliv. 28 (2021) 1342–1355, https://doi.org/10.1080/10717544.2021.1943056.
[13] A. Ashfaq, M.C. Clochard, X. Coqueret, C. Dispenza, M.S. Driscoll, P. Ulanski, M. Al-Sheikhly, Polymerization reactions and modifications of polymers by ionizing radiation, Polymers 12 (2020) 2877, https://doi.org/10.3390/polym12122877.
[14] G. Tamburini, S. Bertagnoli, G. Tarricone, S. Piva, A. Sassella, R. Lorenzi, A. Paleari, Early stages of X-ray induced molecular unit modifications in poly(lactic acid), Polym. Degrad. Stab. 216 (2023) 110485, https://doi.org/10.1016/j.polymdegradstab.2023.110485.
[15] G. Tamburini, G. Tarricone, S. Piva, A. Sassella, S. Bertagnoli, R. Lorenzi, A. Paleari, Tuning crystallinity of poly(L-lactic acid) microspheres through emulsification temperature changes, Macromolecules (2024), https://doi.org/10.1021/acs.macromol.4c01749.
[16] H. Zhang, S. Xiang, Q. Luan, Y. Bao, Q. Deng, M. Zheng, S. Liu, J. Song, H. Tang, F. Huang, Development of poly (lactic acid) microspheres and their potential application in Pickering emulsions stabilization, Int. J. Biol. Macromol. 108 (2018) 105–111, https://doi.org/10.1016/j.ijbiomac.2017.11.079.
[17] P.B. O'Donnell, J.W. McGinity, Preparation of microspheres by the solvent evaporation technique, Adv. Drug Deliv. Rev. 28 (1997) 25–42.
[18] M. Hamoudeh, H. Fessi, H. Salim, Holmium-loaded PLLA nanoparticles for intratumoral radiotherapy via the TMT technique: preparation, characterization, and stability evaluation after neutron irradiation, Drug Dev. Ind. Pharm. 34 (8) (2008) 796–806, https://doi.org/10.1080/03639040801918623.
[19] B. Schrode, S. Pachmajer, M. Dohr, C. Röthel, J. Domke, T. Fritz, R. Resel, O. Werzer, GIDVis: a comprehensive software tool for geometry-independent grazing-incidence X-ray diffraction data analysis and pole-figure calculations, J. Appl. Crystallogr. 52 (2019) 683–689, https://doi.org/10.1107/S1600576719004485.
[20] H.-G. Liu, S. Park, K. Jang, W.-S. Zhang, H.-J. Seo, Y.-I. Lee, Different photoluminescent properties of binary and ternary europium chelates doped in PMMA, Mater. Chem. Phys. 82 (2003) 84–92, https://doi.org/10.1016/S0254-0584(03)00216-5.
[21] K. Binnemans, Interpretation of europium(III) spectra, Coord. Chem. Rev. 295 (2015) 1–45, https://doi.org/10.1016/j.ccr.2015.02.015.
[22] W. Thor, A.N. Carneiro Neto, R.T. Moura Jr., K.-L. Wong, P.A. Tanner, Europium (III) coordination chemistry: structure, spectra and hypersensitivity, Coord. Chem. Rev. 517 (2024) 215927, https://doi.org/10.1016/j.ccr.2024.215927.
[23] R. Ilmi, S. Kansız, N. Dege, M.S. Khan, Synthesis, structure, Hirshfeld surface analysis and photophysical studies of red emitting europium acetylacetonate complex incorporating a phenanthroline derivative, J. Photochem. Photobiol. A Chem. 377 (2019) 268–281, https://doi.org/10.1016/j.jphotochem.2019.03.036.
[24] K. Wasanasuk, K. Tashiro, M. Hanesaka, T. Ohhara, K. Kurihara, R. Kuroki, T. Tamada, T. Ozeki, T. Kanamoto, Crystal structure analysis of poly(L-lactic acid) α form on the basis of the 2-dimensional wide-angle synchrotron X-ray and neutron diffraction measurements, Macromolecules 44 (2011) 6441–6452, https://doi.org/10.1021/ma2006624.
[25] G. Kister, G. Cassanas, M. Vert, Effects of morphology, conformation and configuration on the IR and Raman spectra of various poly(lactic acid)s, Polymer 39 (2) (1998) 267–273, https://doi.org/10.1016/S0032-3861(97)00229-2.
[26] N. Bedoya-Martínez, B. Schrode, A.O.F. Jones, T. Salzillo, C. Ruzié, N. Demitri, Y. H. Geerts, E. Venuti, R.G. Della Valle, E. Zojer, R. Resel, DFT-assisted polymorph identification from lattice Raman fingerprinting, J. Phys. Chem. Lett. 8 (2017) 3690–3695, https://doi.org/10.1021/acs.jpclett.7b01634.
[27] C.Y. Liang, E.J. Schimitschek, J.A. Trias, I.R. and Raman spectra of europium(ill) β-diketonates, J. Inorg. Nucl. Chem. 32 (1970) 811–831.
[28] S.F. Tayyari, F. Milani-nejad, Vibrational assignment of acetylacetone, Spectrochim. Acta A 56 (2000) 2679–2691, https://doi.org/10.1016/S1386-1425(00)00304-8.
[29] R. Bonzanini, E.M. Girotto, M.C. Gonçalves, E. Radovanovic, E.C. Muniz, A. F. Rubira, Effects of europium (III) acetylacetonate doping on the miscibility and photoluminescent properties of polycarbonate and poly(methyl methacrylate) blends, Polymer 46 (2005) 253–259, https://doi.org/10.1016/j.polymer.2004.10.042.
[30] R. Bonzanini, D.T. Dias, E.M. Girotto, E.C. Muniz, M.L. Baesso, J.M.A. Caiut, Y. Messaddeq, S.J.L. Ribeiro, A.C. Bento, A.F. Rubira, Spectroscopic properties of polycarbonate and poly(methyl methacrylate) blends doped with europium (III) acetylacetonate, J. Lumin. 117 (2006) 61–67, https://doi.org/10.1016/j.jlumin.2005.04.010.
[31] P. Ekholm, L. Virkki, M. Ylinen, L. Johansson, P. Varo, Effects of natural chelating agents on the solubility of some physiologically important mineral elements in oat bran and oat flakes, Cereal Chem. 77 (5) (2000) 562–566, https://doi.org/10.1094/CCHEM.2000.77.5.562.
[32] J. Stary, J.O. Liljenzin, Critical evaluation of equilibrium constants involving acetylacetone and its metal chelates, Pure Appl. Chem. 54 (1982) 2557–2592, https://doi.org/10.1351/pac198254122557.
[33] S. Teixeira, K. Morawa Eblagon, F. Miranda, M. Fernando, R. Pereira, J. L. Figueiredo, Towards controlled degradation of poly(lactic), Acid Tech. Applic. C 7 (2021) 42, https://doi.org/10.3390/c7020042.
[34] P. Stanley May, F.S. Richardson, Non-radiative deactivation of the europium 5D0 excited state by water molecules outside the primary coordination sphere of Eu3+ in Na [Eu(C4H4O5)3]2NaClO4 6H2O, Chem. Phys. Lett. 179 (1991) 277–281.
[35] J. Salaam, I. N'Dala-Louika, C. Balogh, I. Suleimanov, G. Pilet, L. Veyre, C. Camp, C. Thieuleux, F. Riobé, O. Maury, Tris-dipicolinate lanthanide complexes: influence of the second hydration sphere on the solid-state luminescence properties, Eur. J. Inorg. Chem. (2022) e202200412, https://doi.org/10.1002/ejic.202200412.
[36] J.-S. Yoon, H.-W. Jung, M.-N. Kim, E.-S. Park, Diffusion coefficient and equilibrium solubility of water molecules in biodegradable polymers, J. Appl. Polym. Sci. 77 (2000) 1716–1722.
[37] P. Mandal, J. Kretzschmar, B. Drobot, Not just a background: pH buffers do interact with lanthanide ions - a Europium(III) case study, JBIC J. Biol. Inorg. Chem. 27 (2022) 249–260, https://doi.org/10.1007/s00775-022-01930-x.
[38] L. Labrador-Páez, M. Pedroni, P. Haro-González, E. Camarillo, M. Bettinelli, D. Jaque, J. García-Solé, Eu3þ luminescent ions detect water density anomaly, J. Lumin. 223 (2020) 117263, https://doi.org/10.1016/j.jlumin.2020.117263.